

## Nontrivial spin structure of graphene on Pt(111) at the Fermi level due to spin-dependent hybridization

I. I. Klimovskikh,<sup>1</sup> S. S. Tsirkin,<sup>2,3</sup> A. G. Rybkin,<sup>1</sup> A. A. Rybkina,<sup>1</sup> M. V. Filianina,<sup>1</sup>  
E. V. Zhizhin,<sup>1</sup> E. V. Chulkov,<sup>2,4</sup> and A. M. Shikin<sup>1</sup>

<sup>1</sup>*Saint Petersburg State University, Saint Petersburg 198504, Russia*

<sup>2</sup>*Donostia International Physics Center (DIPC), 20018 San Sebastián/Donostia, Basque Country, Spain*

<sup>3</sup>*Tomsk State University, 634050 Tomsk, Russian Federation*

<sup>4</sup>*Departamento de Física de Materiales UPV/EHU, Centro de Física de Materiales CFM - MPC  
and Centro Mixto CSIC-UPV/EHU, 20080 San Sebastián/Donostia, Basque Country, Spain*

(Received 24 September 2014; revised manuscript received 17 November 2014; published 22 December 2014)

The electronic and spin structure of a graphene monolayer synthesized on Pt(111) has been investigated experimentally by angle- and spin-resolved photoemission with different polarizations of incident synchrotron radiation and using density functional theory calculations. It is shown that despite the observed total quasifreestanding character of the dispersion of the graphene  $\pi$  state remarkable local distortions and breaks in the dispersions take place due to hybridization between the graphene  $\pi$  and Pt  $d$  states. Corresponding spin-dependent avoided-crossing effects lead to significant modification of the spin structure and cause an enhanced induced spin-orbit splitting of the graphene  $\pi$  states near the Fermi level in the region of the  $\bar{K}$  point of the graphene Brillouin zone (BZ) with a magnitude of 80–200 meV depending on the direction in the BZ. Using  $p$ ,  $s$ , and elliptical polarizations of the synchrotron radiation, the contributions of the graphene  $\pi$  and Pt  $d$  states were separated and their intersection at the Fermi level, which is important for effective spin injection between these states, was shown. Moreover, analysis of the data allows us to conclude that in the region of the Dirac point the spin structure of the system cannot be described by a Rashba splitting, and even a spin-orbit gap between lower and upper Dirac cones is observed.

DOI: [10.1103/PhysRevB.90.235431](https://doi.org/10.1103/PhysRevB.90.235431)

PACS number(s): 73.22.Pr, 75.70.Tj

### I. INTRODUCTION

It is well known that due to the linear dispersion of the  $\pi$  states near the Fermi level graphene is characterized by unique properties such as zero effective mass of Dirac fermions, high speed of electrons at the Fermi level, and ultrahigh group velocity [1–4]. This makes graphene an indispensable material for the further development of nanoelectronics. Moreover, owing to the large spin-relaxation length, it can be effectively used in spintronics as a material for graphene spin filters and for graphene field-effect transistors [5–9]. However, up to now graphene is used in spintronics only as a passive element due to the low magnitude of the spin-orbit splitting of graphene  $\pi$  states. In particular, in the graphene spin filter it is used as a passive element, only for effective transport of spin current injected between two ferromagnetic (FM) electrodes. Nevertheless, recent series of works [10–12] demonstrate that interaction of graphene with intercalated heavy  $d$  metals such as Au leads to an enhanced spin-orbit splitting of the graphene  $\pi$  states near the Fermi level in the region of the  $\bar{K}$  point of the Brillouin zone (BZ). It was shown that this effect is mainly determined by the hybridization between the  $d$  states of Au and  $\pi$  states of graphene and corresponding spin-dependent avoided-crossing effects involving these states. Such spin splitting of the  $\pi$  state allows the use of graphene not only for spin transport devices, but assumes a possibility to utilize it as an element of the spin injector, i.e., as an active element in spintronics. However, if intercalated metals have lower atomic number, e.g., Cu, the value of the spin splitting is negligible despite having similar effects of hybridization between the graphene  $\pi$  and metal  $d$  states [10]. It is noteworthy that intercalation of heavy metal Bi with the  $sp$ -type valence band

under graphene does not lead to remarkable spin-orbit splitting of the  $\pi$  state of graphene. It means that a search for appropriate metals providing a high value of the spin-orbit splitting of the graphene  $\pi$  states is a very important problem for the effective use of graphene in spintronics.

Furthermore, it is noteworthy that for spintronics an efficiency of using of the graphene/Au interface for the spin current formation can be significantly limited because the Au  $d$  states have binding energies of more than 2.5 eV below the Fermi level. This prevents Au  $d$  states from participation in the spin transport and spin injection phenomena. In this respect other heavy  $d$  metals with localization of the  $d$  states near the Fermi level, such as Ir, Re, or Pt, should be more suitable materials, which can resolve the problem of passing spin currents from graphene in designing corresponding spin devices. Unfortunately, graphene on Re(0001) is characterized by strong hybridization with the substrate, followed by significant distortion of the graphene Dirac cone structure [13], and therefore cannot be used for such application. Graphene on Ir(111) is characterized by the Dirac cone structure of the graphene  $\pi$  state at the Fermi level. Moreover, recently the spin splitting of the  $\pi$  state of graphene on Ir(111) was demonstrated [14]. However, the electronic structure of Ir(111) is characterized by a local gap in the region  $\bar{K}$  point of graphene, and a hybridization between the Ir  $d$  and graphene  $\pi$  states takes place significantly below the Fermi level. As in the case of interaction of graphene with Au it does not assume an effective spin injection between the graphene  $\pi$  states and  $d$  states of metal at the Fermi level.

The current work is devoted to a detailed investigation of the features of electronic and spin structure of the graphene/Pt interface and corresponding spin-dependent avoided-crossing

effects, especially in the region of the crossing between the Pt and graphene  $\pi$  states at the Fermi level near the  $\bar{K}$  point of the BZ with the perspective of using this structure for the creation of the spin current. On the one hand, platinum is a heavy  $d$  metal promising an enhanced interatomic potential gradient that is necessary for enhanced spin orbit splitting in the graphene  $\pi$  states, which is assumed to be induced due to interaction with the Pt  $d$  states similar to the case of the contact of graphene with Au [10–12]. Moreover, in accordance with Refs. [15,16], the bonding of graphene synthesized on Pt(111) with the substrate weak. This means that the contact with Pt is not expected to lead to significant distortions of the electronic structure of graphene. On the other hand, the Pt valence-band  $d$  states are localized near the Fermi level that allows us to realize an effective spin transport between graphene and Pt. Due to a high density of the  $5d$  states at the Fermi level Pt is characterized by a large spin Hall effect [17,18] that allows us to use Pt widely in spintronics as a detector of the spin accumulation or for the corresponding spin current formation; see, for instance Refs. [19,20]. It is often used as a material for effective conversion of the spin current into induced magnetization of ferromagnetic layers due to the spin torque effect [21,22].

In the present work the spin electronic structure of graphene synthesized on Pt(111) has been investigated by means of angle- and spin-resolved photoemission spectroscopy with the  $p$ ,  $s$ , and elliptic polarizations. We have studied the features of electronic structure, developed under contact of graphene with the Pt(111) substrate, in particular the behavior of the  $\pi$  state of graphene and  $d$  states of Pt near the Fermi level. We present the DFT calculation results for the electronic and spin structure of a graphene monolayer on Pt(111) and compare them with the experimental findings. Finally, based on the results, we analyze the formed spin structure, and estimate the opportunity of the application of a graphene/Pt interface in spintronics.

## II. EXPERIMENTAL AND COMPUTATIONAL DETAILS

The experiments were carried out at Helmholtz-Zentrum Berlin (BESSY II) at beamlines UE112-SGM and U125/2-SGM with the assistance of a Scienta R4000 energy analyzer using linearly and circularly polarized synchrotron radiation. The spin-resolved photoemission spectra were measured using a Mott spin detector operated at 26 keV. Total-energy resolution during experiments was 50 meV. The spin- and angle-resolved photoemission spectroscopy (SARPES) measurements were carried out with the angular resolution of  $1^\circ$ , that corresponds to a momentum resolution of  $0.07 \text{ \AA}^{-1}$  at a photon energy of 62 eV. The measurable spin splitting is not limited by the energy resolution, but rather by the acquired statistics. Our estimations of splittings between the resolved features were derived from the fitting of the spectrum features and from the procedures, described in Ref. [23]. The angle of the synchrotron radiation incidence was  $45^\circ$  relative to the surface normal for the normal emission measurements. Measurements of the dispersion relations with  $E(k_{\parallel})$  were carried out by tilting the sample in the plane perpendicular to the plane of polarization of the incident synchrotron radiation. The  $p$ -polarized undulator radiation was used with orientation

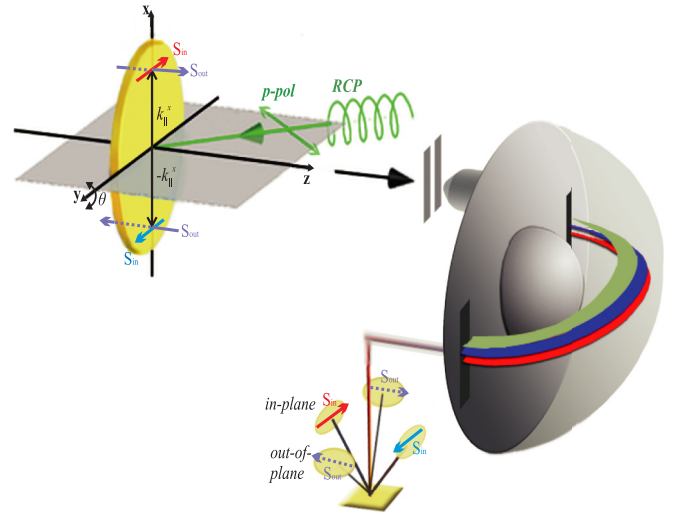


FIG. 1. (Color online) Schematic drawing of the geometry of the experiment. Variation of  $k_{\parallel}$  across the whole BZ takes place by rotating of the sample in the two planes. The  $p$ ,  $s$ , and circular polarization of the incident radiation is used. The measured in-plane orientation of spin is parallel to the plane of the light polarization.

of the polarization plane parallel to the orientations of spin of the studied states (which is locked perpendicular to momentum). Therefore, the variation of the tilt angle (corresponding to the variation of  $k_{\parallel}$ ) took place in the plane perpendicular to the plane of the incident light polarization, parallel to the slit of the analyzer. The schematic drawing of the geometry of the experiment is shown in Fig. 1. For the measurements with circular polarization (clockwise and anticlockwise) of the incident light the same geometry of the experiment was used. Part of the experiments were performed out in Research Resource Center of Saint Petersburg State University “Physical methods of surface investigation” with the same geometry of the experiment using a monochromatized discharge He lamp. A part of the spin-resolved experiment was carried out using the geometry with the orientation of spin perpendicular to the light polarization plane, as will be explained below. A clean surface of Pt(111) was prepared by repeated cycles of Ar sputtering and annealing at 1300 K. The crystalline order and cleanliness of the surface were verified by low-energy electron diffraction (LEED) and x-ray photoemission spectroscopy (XPS). The graphene monolayer was synthesized at Pt(111) by cracking of the propylene ( $C_3H_6$ ) at a pressure of  $1 \times 10^{-7}$  mbar and a sample temperature of 1200 K during 60 min.

Density functional theory (DFT) calculations of the electronic structure and spin polarization of a graphene monolayer on Pt(111) were performed using the VASP code [24,25], following the projector-augmented wave (PAW) method [26,27] with the generalized gradient approximation of Perdew, Burke, and Ernzerhof (GGA-PBE) [28], which is applied in order to represent the exchange-correlation energy. The spin-orbit interaction (SOI) is described within the second variation method [29]. Van der Waals interactions are taken into account within the DFT-D2 approach [30]. The calculations were performed in a slab geometry: the slab consisted of 14 atomic layers of Pt(111) with a graphene monolayer placed on one

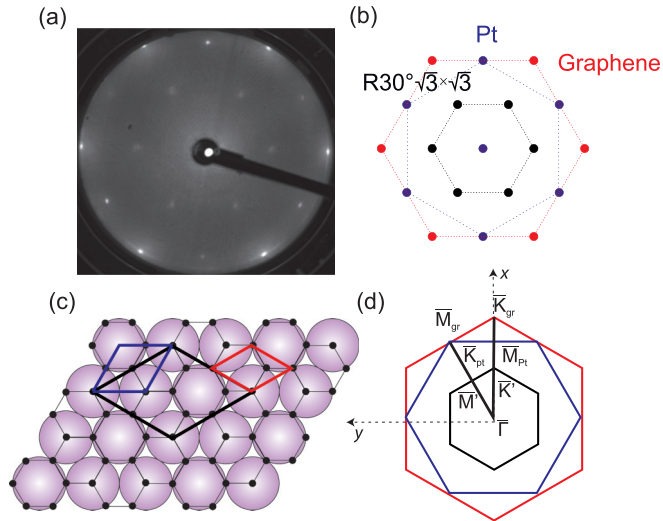


FIG. 2. (Color online) LEED pattern for graphene on Pt(111) with at  $E_p = 82$  eV (a) with simulation of the contributions for the graphene and Pt(111) structural cells (b), shown by red and blue colors, respectively. (c) Top view of mutual atomic arrangement in graphene and Pt layers. The  $2 \times 2$  supercell of graphene is shown by black color. (d) The mutual arrangement of the graphene and Pt(111) Brillouin zone. Axes  $x$  and  $y$  are directed along  $\bar{\Gamma}\bar{K}$  and  $\bar{\Gamma}\bar{M}$  directions of BZ of graphene, respectively.

side of the slab as shown in Fig. 2(c), while the other side is covered with hydrogen. Hydrogen was included to prevent formation of surface states on that side, which could lead to artificial splitting of surface states due to finite slab thickness. The position of the atoms in graphene and four neighboring layers of Pt were relaxed to their equilibrium positions, while the other layers of Pt were fixed at their bulk positions. The calculated distance between the graphene layer and the Pt surface atomic layer is 3.16 Å, and the first and the second Pt(111) interlayer spacings show small expansions of 4% and 2%, respectively. The resulting structure of the graphene monolayer is close to the ideal  $1 \times 1$  structure, both the lateral and in-plane shifts of atoms being less than  $10^{-2}$  Å.

### III. RESULTS

Figure 2(a) presents LEED pattern for graphene synthesized on Pt(111) by the method described above which was measured at the primary electron beam energy  $E_p = 82$  eV. Corresponding simulation of the LEED pattern with the contributions from the graphene and Pt(111) surfaces is shown in Fig. 2(b). A schematic presentation of the BZ of graphene and Pt(111) is presented in Fig. 2(d). The LEED pattern is formed by three kinds of hexagonal lattices, corresponding to the graphene lattice, the platinum lattice and the  $(\sqrt{3} \times \sqrt{3})R30^\circ$  superstructure relative to Pt(111). Graphene hexagon in the formed structure is rotated by  $30^\circ$  relative to the Pt(111)-derived structures. Hence, the  $\bar{\Gamma}\bar{K}$  direction in the BZ of graphene corresponds to the  $\bar{\Gamma}\bar{M}$  direction in the surface Brillouin zone (SBZ) of Pt(111) and vice versa. Relative to the graphene structure, the formed supercell can be considered as a  $(2 \times 2)$  structure. The corresponding arrangement of atoms in the graphene layer relative to the Pt(111) surface is shown

in Fig. 2(c). According to the LEED pattern, graphene forms a well-ordered structure with one preferential orientation of the formed graphene domains. Meanwhile the domains with the orientations rotated by  $30^\circ$  can be also distinguished by LEED due to the tails of some ringlike stripes oriented along the main graphene reflexes. Note that the size of domains of graphene on Pt(111) with different orientations strongly depends on parameters of synthesis. In addition to the  $30^\circ$  domain, varying the temperature of sample and exposure of propylene we observed the formation of the domains with the structures rotated on  $0^\circ$  and  $19^\circ$  relative to Pt(111), in agreement with previous works [16,31,32].

Figures 3(a) and 3(b) show the dispersion relations of the valence-band electronic states for graphene monolayer synthesized at Pt(111) measured in the  $\bar{\Gamma}\bar{M}$  (a) and  $\bar{\Gamma}\bar{K}$  (b) directions of the graphene BZ, respectively. The measurements were carried out at room temperature at photon energy of 52 eV. Figure 3(c) represents the theoretical spin-density distribution of the graphene-derived electronic states in the  $\bar{\Gamma}\bar{K}$  direction, assuming the  $(\sqrt{3} \times \sqrt{3})R30^\circ$  structure of graphene relative to platinum. The presented experimental dispersion relations are characterized by a pronounced branch of the graphene  $\pi$  states which cross the Fermi level near the  $\bar{K}$  point of the graphene BZ at  $k_x = 1.7 \text{ \AA}^{-1}$ . In order to distinguish the directions of the dispersion dependencies in the BZ along the  $\bar{\Gamma}\bar{K}$  and perpendicular to the  $\bar{\Gamma}\bar{K}$  directions (through the  $\bar{K}$  point) we introduce the notation  $k_x$  (along  $\bar{\Gamma}\bar{K}$ ) and  $k_y$  (perpendicular to  $\bar{\Gamma}\bar{K}$ ). At the  $\bar{\Gamma}$  point the  $\pi$  states have the binding energy (BE) of 8.2 eV. Besides the main branch of the graphene  $\pi$  states the theoretical calculations in Fig. 3(c) show additional folded branches which are formed due to the  $(2 \times 2)$  superstructure of graphene. They do not display themselves in the experimental data due to the reduced value of corresponding matrix elements. In the  $\bar{\Gamma}\bar{M}$  direction the  $\pi$  state reaches an energy of 3 eV at  $k_y = 1.4 \text{ \AA}^{-1}$  that corresponds to the  $\bar{M}$  point of the BZ of graphene. Besides the  $\pi$  states, Figs. 3(a) and 3(b) display dispersions of the graphene  $\sigma$  states which have a binding energy of about 4.5 eV in the  $\bar{\Gamma}$  point and are dispersing toward the higher binding energies with increasing  $k_{\parallel}$  in both the  $\bar{\Gamma}\bar{K}$  and  $\bar{\Gamma}\bar{M}$  directions. In Fig. 3(c) the  $\sigma$  states cannot be distinguished, because these states are not spin polarized.

In Figs. 3(a) and 3(b) one can also distinguish additional branches of the  $\pi$  states, corresponding to the graphene domains, rotated by  $30^\circ$  relative to the main domains. These branches have low intensity. On the presented dispersions they manifest themselves as additional weak branches which have maximal BE of about 3 eV in the  $\bar{\Gamma}\bar{K}$  direction and reach the Fermi level under measurements in the  $\bar{\Gamma}\bar{M}$  direction.

In addition to the graphene-derived states the presented dispersions are characterized by a series of branches of the Pt 5d states. These states are localized in the BE region between the Fermi level and 3 eV and are marked in Fig. 3 as Pt  $d$ . At the  $\bar{\Gamma}$  point the Pt 5d states have energies of 0.1, 0.9, and 1.8 eV, which correlate with the energies of the  $d$  states of Pt(111) surface [33,34]. For more detailed information about the behavior of Pt  $d$  states and their interaction with  $\pi$  state of graphene the photoemission measurements with opposite circular polarization of the incident synchrotron radiation were carried out. The dispersion relations of graphene on

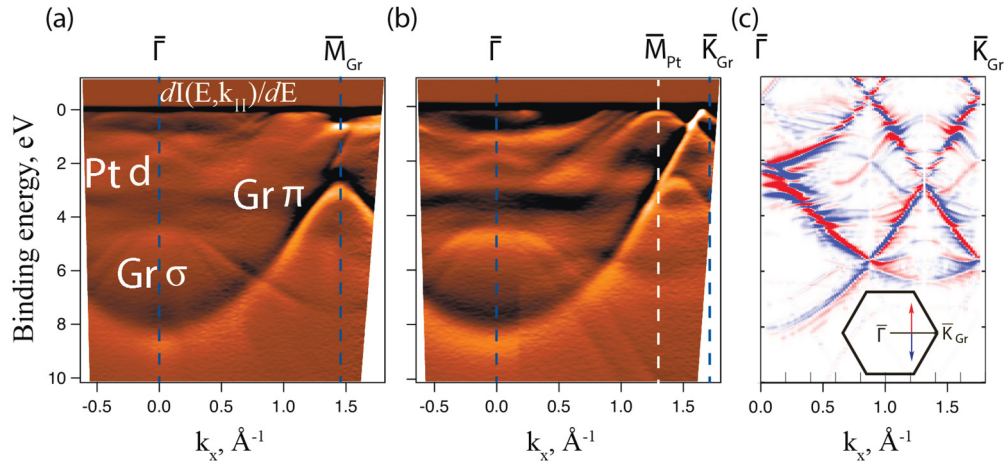


FIG. 3. (Color online) Experimental dispersion relations of electronic states of MG/Pt(111) in the  $\bar{\Gamma}\bar{M}$  (a) and  $\bar{\Gamma}\bar{K}$  (b) directions of the BZ of the graphene. (c) The calculated  $k$ -resolved local spin density of graphene in the  $\bar{\Gamma}\bar{K}$  direction. The red and blue colors correspond to different directions of spin polarization, as denoted by the arrows in the inset.

Pt(111) measured along the  $\bar{\Gamma}\bar{K}$  direction in the region of the  $\bar{K}$  point, with positive and negative (clockwise and anticlockwise, respectively) elliptic polarizations, are shown in Figs. 4(c) and 4(d). For better visualization the second derivatives  $d^2I(E, k_{||})/d^2E$  are presented. In Fig. 4(a) the detailed dispersion relations in the same region measured at 18 K for the same system with the linear  $p$  polarization are shown, for comparison. The positions of the  $\bar{K}$  point in the graphene BZ and the  $\bar{M}$  point in the Pt(111) SBZ are denoted by white dashed lines in the figures.

As shown in Fig. 4(a), the set of branches of the Pt  $d$  states, marked as  $\alpha$ ,  $\beta$ , and  $\gamma$ , are shifting to the Fermi level with  $k_x$ , crossing it near the  $\bar{M}$  point of the SBZ of Pt and

going out to the region of unoccupied states above the Fermi level. The  $\bar{M}$  point of the SBZ of Pt is located along the  $\bar{\Gamma}\bar{K}$  direction of the BZ of graphene at  $k_x = 1.3 \text{ \AA}^{-1}$ . With further increase of  $k_x$ , under transition to the second SBZ of Pt, the branches of Pt  $d$  states are shifting back to the occupied states below the Fermi level and cross the branch of the  $\pi$  state of graphene. Intersection of the branches  $\alpha$  and  $\beta$  with the  $\pi$  state takes place at the energy of 0.7–0.9 eV, and with the branch  $\gamma$  at the Fermi level. In Fig. 4(a) the weaker branch of the Pt  $d$  states, localized between  $\beta$  and  $\gamma$ , can be also resolved, but in the second BZ of Pt it is not visible. This behavior of the  $d$  states of Pt correlate with that observed for a pure surface of Pt(111), for example see Refs. [33,34]. In Figs. 4(c) and 4(d)

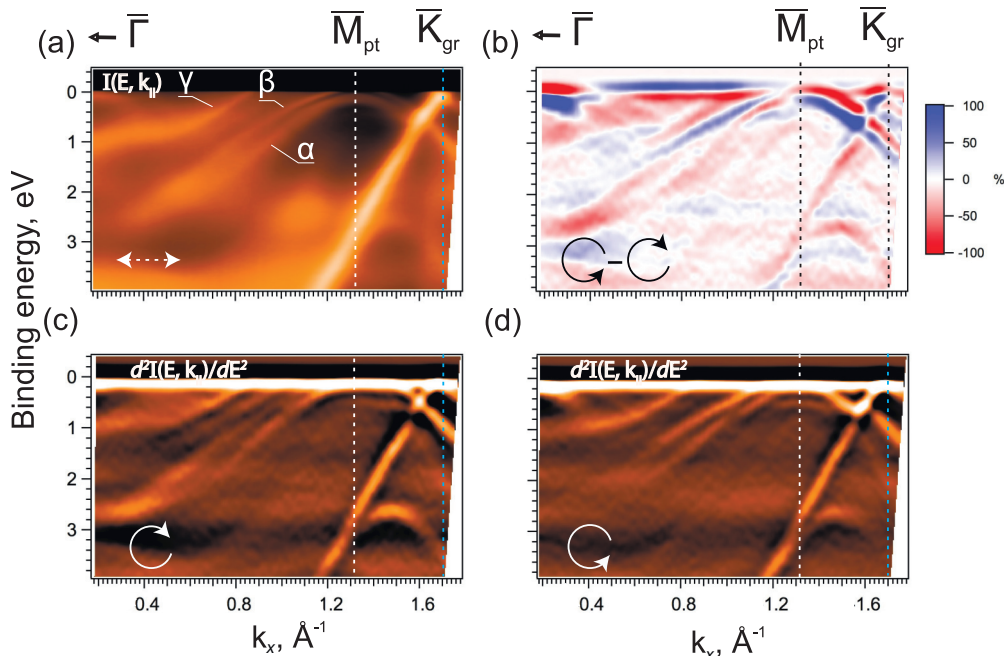


FIG. 4. (Color online) (a) Experimental dispersion relations of electronic states of MG/Pt(111) taken at 18 K with  $p$ -polarized light. Photon energy is 62 eV. Second derivatives of photoemission intensity using clockwise (c) and anticlockwise (d) circular polarized radiation, and their difference (b).

two pronounced crossings of the  $d$  states of Pt and the  $\pi$  state of graphene can be clearly distinguished at  $k_x = 1.6 \text{ \AA}^{-1}$  and at the  $\bar{K}$  point of graphene, at  $k_x = 1.7 \text{ \AA}^{-1}$ , where a significant distortion of the dispersions are indeed observed. It is clearly seen that near the crossing points the behavior of the  $\pi$  state of graphene deviates from the linear one. At  $k_x = 1.5 \text{ \AA}^{-1}$  the intensity of the  $\pi$  state is significantly weakened, and at  $k_x = 1.6\text{--}1.7 \text{ \AA}^{-1}$  kinks of the  $\pi$  state and mixing with the Pt states are observed. These observations are related to the hybridization between the involved states.

For better visualization the difference profiles were constructed as subtraction of the second derivatives of the photoemission intensity shown in Figs. 4(c) and 4(d). The resulting image is presented in Fig. 4(b). Here, the negative difference in the intensities characterized by dominant contribution of the features with clockwise polarization of light is shown by red color. The positive difference in the intensities corresponding to anticlockwise polarization is shown by blue color. The different influences of opposite directions of the circular polarization of light on the photoemission spectra can be related to sensitivity to details of the spin-dependent hybridization. According to the avoided-crossing effect each  $\pi$  state interacts with a Pt  $d$  states with parallel orientation of spin. As a result, formation of the local distortions in the electronic structure and significant modification of the spin structure takes place. Red and blue colors in the dispersions of the Pt  $d$  states indicate strong spin-orbit interaction. Hybridization of the spin-orbit split Pt  $d$  states and the  $\pi$  state of graphene leads to changes not only in character of dispersion, but also in spin structure of the  $\pi$  state of graphene. The splitting of the  $\pi$  states can be distinguished in the region of intersection with the Pt  $d$  states. Of course, Fig. 4(b) cannot be the direct evidence of the spin polarization of  $\pi$  state, since the circularly polarized light interacts with the spin of electron via orbital momentum, and strongly depends on photon energy and the geometry of the experiment. However, taking into account the spin-dependent hybridization between clearly resolved spin split Pt  $d$  states and the graphene  $\pi$  state we can conclude that the spin structure of the  $\pi$  state is modified under interaction with Pt with possible spin splitting of the graphene at the Fermi level. For a direct study of the spin structure the direct spin measurements using a Mott detector are required.

In order to investigate more clearly the character of the dispersion of the graphene  $\pi$  states we have measured the dispersion through the  $\bar{K}$  point of the BZ but in the direction perpendicular to the  $\bar{\Gamma}\bar{K}$ . To distinguish the contributions of the graphene and Pt  $d$  states we have also used the different ( $p$  and  $s$ ) polarization of light. With this geometry of the experiment with use of the  $p$  polarization of light the graphene  $\pi$  states have dominant contributions in the spectra.

Figure 5(a) indicates clearly that the dispersion of the graphene  $\pi$  state near the  $\bar{K}$  point of the graphene BZ measured with  $p$  polarization of light has a pronounced linear character. The linear character of the dispersion of the graphene  $\pi$  states on Pt(111) was also noted in Ref. [16]. It is similar to that observed for the system graphene on Ni(111) after intercalation of a Au monolayer [8,10–12,35,36] as an example of generally weak interaction at graphene-noble metal interfaces. The Dirac point for the graphene/Pt system, corresponding to the crossing between the Dirac cones of the

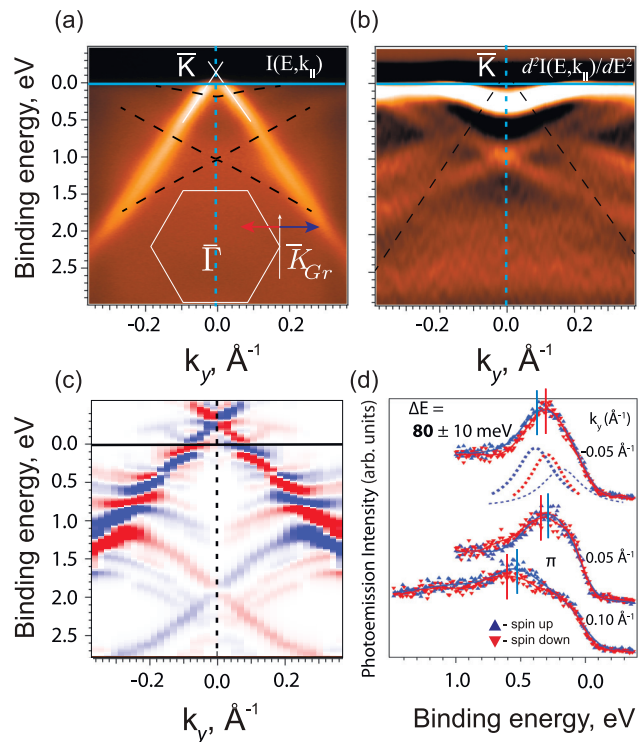


FIG. 5. (Color online) Experimental dispersion relations of electronic states of MG/Pt(111) in the direction, perpendicular to  $\bar{\Gamma}\bar{K}$  with using the  $p$ -polarized (a) and  $s$ -polarized light (b). Black dashed lines show schematic dispersion of Pt (a) and graphene (b) states. (c) The calculated  $k$ -resolved local spin density of graphene in the direction perpendicular to  $\bar{\Gamma}\bar{K}$ . The red and blue colors correspond to different directions of spin polarization, as shown by arrows in the inset. (d) Experimental spin-resolved ARPES spectra for various emission angles in the direction perpendicular to  $\bar{\Gamma}\bar{K}$ .

$\pi$  and  $\pi^*$  states, is located slightly above the Fermi level. Our approximation of the linear dependencies of  $\pi$  states from both sides of the  $\bar{K}$  point gives a value of an energy of the Dirac point position of about 150 meV above the Fermi level while the DFT calculation yields a slightly higher value.

Meanwhile, we have to note that despite a total quasifree-standing character of the graphene  $\pi$ -state dispersion, a local distortion of the dispersion relations of the graphene  $\pi$  state at intersections with Pt  $5d$  states takes place as demonstrated in Fig. 3(a). In order to separate the contributions of the Pt  $5d$  and the graphene  $\pi$  states in the region of the  $\bar{K}$  point, the dispersions measured in the same energy and  $k_y$  regions as in Fig. 5(a), but with use of the  $s$  polarization, are shown in Fig. 5(b). These spectra show mainly the contribution of the Pt  $5d$  states. The graphene  $\pi$  states are practically nonvisible in this case. As we can see from Fig. 5(b), two pronounced branches of the Pt  $d$  states cross the  $\pi$  states of graphene near the  $\bar{K}$  point: the first one near the Fermi level and the second one at 0.7 eV. These features are annotated also in Fig. 5(a) by the black dashed lines. Pt  $d$  states with the highest intensity in the region of the  $\bar{K}$  point are located just at the Fermi level (that is important for a possibility of the spin injection between the graphene and Pt  $d$  states at the Fermi level). This result correlates with the dispersion relations presented in Fig. 3(a)

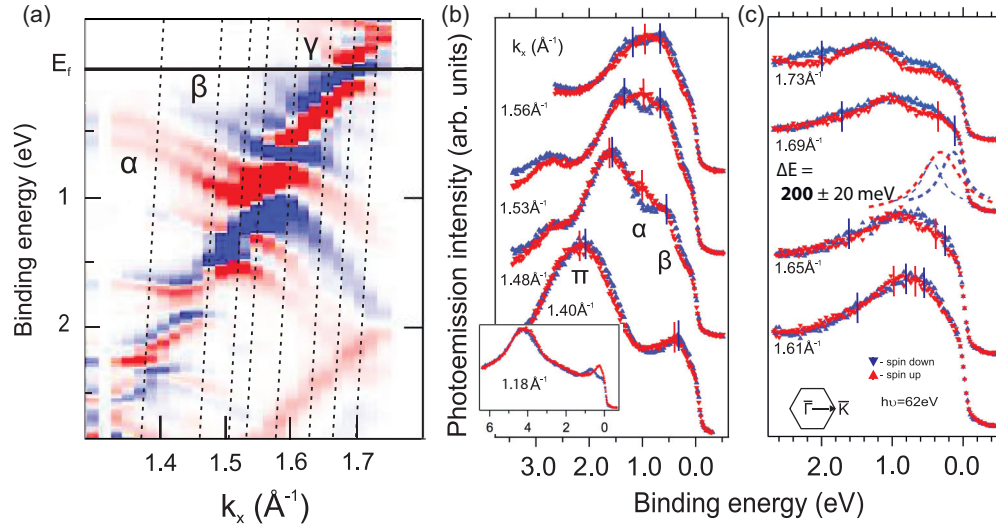


FIG. 6. (Color online) (a) The calculated  $k$ -resolved local spin density of graphene on Pt(111) in the  $\bar{\Gamma}\bar{K}$  direction in the region of  $\bar{K}$  point of BZ of graphene. Dashed lines represent corresponding emission angles, which were used for spin-resolved photoemission spectra. Experimental spin-resolved data for the series of emission angle (b) and (c). Red and blue color have the same meaning as in Fig. 3(c). At the inset additional spectrum with  $k_{\parallel} = 1.18 \text{ \AA}^{-1}$  is presented. This part of spin-resolved data was measured with the orientation of spin perpendicular to the light polarization plane.

where we can see the crossing between the graphene  $\pi$  states and the Pt  $5d$  states at these energies. With shifting  $k_y$  from the  $\bar{K}$  point these branches disperse symmetrically to higher and to lower binding energies. Partially the Pt  $d$  states can be resolved in Fig. 5(a) but at these conditions they have significantly lower intensity than the  $\pi$  states of graphene.

As we noted above, the intersection of graphene  $\pi$  states with Pt  $5d$  states in the region of the  $\bar{K}$  point leads to hybridization between the graphene  $\pi$  state and Pt  $5d$  states and corresponding spin-dependent avoided-crossing effects between these states. Similar effects were observed for interaction of  $\pi$  state with Au  $d$  states when the monolayer of Au was intercalated underneath graphene [8,11,36]. It is assumed by analogy that the spin-dependent hybridization between the Pt  $d$  and graphene  $\pi$  states should lead to significant modification of the electronic and spin structures of the graphene  $\pi$  states and their induced spin-orbit splitting.

The DFT calculations of the spin-density distribution, presented in Fig. 5(c) for the direction, perpendicular to  $\bar{\Gamma}\bar{K}$ , show the significant influence of spin-dependent avoided-crossing effects under interaction of the graphene  $\pi$  states with spin-polarized Pt  $d$  states. Therefore, at the Fermi level near the  $\bar{K}$  point of the BZ of graphene a pronounced spin polarization of the graphene  $\pi$  states is clearly visible. The value of the spin splitting of the graphene  $\pi$  states at the Fermi level reaches 100 meV. Note that the sign of the spin polarization of the graphene  $\pi$  states is inverted relative to the  $\bar{K}$  point. The quantization axis in the calculations and measurements of the spin polarization are always oriented perpendicular to momentum, i.e., for nonzero  $k_x$  it is along the  $y$  axis and vice versa.

Figure 5(d) shows the experimental spin-resolved photoemission spectra at various emission angles, measured in the direction perpendicular to the  $\bar{\Gamma}\bar{K}$  on both sides from the  $\bar{K}$  point. With this geometry the contribution of the  $\pi$  states dominates in the photoelectron spectra. However, the Pt  $d$  state

near the Fermi level introduces additional spin polarization and asymmetry of the spin splitting. Thus, taking into account the contribution of the Pt  $d$  states near the Fermi level [see, for comparison Fig. 5(b)] for fitting of the spectrum near the  $\bar{K}$  point we used one spin-up and two spin-down peaks, as shown in Fig. 5(d). From analysis of the presented data, we can see that the value of the spin splitting of the  $\pi$  state of graphene at the Fermi level is  $80 \pm 10$  meV. With shifting from the  $\bar{K}$  point toward the place of intersection with other branches of the Pt  $d$  states the value of the splitting increases, in accordance with theoretical calculations, due to pronounced spin-dependent avoided-crossing effects. The sign of the spin polarization is antisymmetric relative to the  $\bar{K}$  point.

For a detailed analysis of the spin structure of the MG/Pt(111) interface along the  $\bar{\Gamma}\bar{K}$  direction of the BZ of graphene, the results of the DFT calculations of the spin density distribution of states, localized at the graphene layer in the region near the  $\bar{K}$  point, are presented in Fig. 6(a). Evidently, the linear dispersion of the  $\pi$  state of graphene can be rather seen as an envelope function of maxima of spin density. The branches of the strongly spin-polarized Pt  $d$  states  $\alpha$  and  $\beta$  are shown as low-intensity features, dispersing from the  $\bar{M}$  point of the Pt SBZ to higher binding energy. State  $\beta$  represents a spin-down surface  $d$  resonance, while  $\alpha$  consists of two spin-up states. In the region of  $k_x = 1.5\text{--}1.65 \text{ \AA}^{-1}$  a significant modification of the spin structure takes place, due to hybridization with the  $\pi$  state of graphene and corresponding spin-dependent avoided-crossing effect. Similar effects of strong modification of the spin structure of the graphene  $\pi$  states under intersection with weaker branches of the Pt  $d$  states are also observed in regions with higher BE. However, the most important feature of the calculated spin structure is a pronounced spin-orbit splitting of the graphene  $\pi$  state observed near the Fermi level in the region close to the  $\bar{K}$  point, which takes place as a result of the hybridization. The value of the spin-orbit splitting of the graphene  $\pi$  states near the

Fermi level reaches the magnitude of 150–200 meV. Hence, in the region of  $k_x = 1.6\text{--}1.7 \text{ \AA}^{-1}$  we can distinguish practically linearlike dispersion of the spin-split  $\pi$  state of graphene. At the Fermi level the intersection with the  $\gamma$  state takes place, and a small kink of the  $\pi$  state also takes place. As we can see from Fig. 6(a), the spin splitting of the  $\pi$  state is observed not only in the regions described above but also at  $k_x = 1.3\text{--}1.5 \text{ \AA}^{-1}$ , where hybridization with the Pt  $d$  states also occurs.

In order to confirm the conclusions made above, the direct measurements of the spin structure with a Mott detector were carried out. Figures 6(b) and 6(c) represents a set of photoelectron spectra with spin resolution for a series of the polar angle corresponding to the region of  $k_x = 1.4\text{--}1.73 \text{ \AA}^{-1}$  relative to the surface normal, measured in the  $\bar{\Gamma}\bar{K}$  direction of the BZ of graphene. The dotted lines in Fig. 6(a) correspond to the polar angles, used for measurements of the spin-resolved data, presented in Figs. 6(b) and 6(c).

As can be seen from the experimental spectra, the  $\pi$  state of graphene in the region of crossing with Pt  $d$  states are actually spin split. Spin polarization of the Pt  $d$  states  $\alpha$  and  $\beta$  is clearly visible at  $k_x = 1.40\text{--}1.53 \text{ \AA}^{-1}$ . The spin splitting of the  $\pi$  state can be clearly distinguished for this region. The value of the splitting at  $k_x = 1.4 \text{ \AA}^{-1}$  is around 80 meV. The pronounced intersection between the graphene  $\pi$  state and Pt  $d$  states  $\alpha$  and  $\beta$  takes place at a value of  $k_x$  around  $1.6 \text{ \AA}^{-1}$ . With further increasing  $k_{\parallel}$ , the graphene  $\pi$  state approaches the Fermi level, and the Pt  $d$  states are shifted to the higher binding energies in accordance with theoretical calculations. Despite a significant masking influence of the Pt  $d$  states the spin splitting of the  $\pi$  state of graphene can be clearly distinguished near the Fermi level. The splitting of  $\pi$  state of graphene near the  $\bar{K}$  point is  $200 \pm 20$  meV. For fitting of the spectra we use a set of spin-polarized Pt peaks and two spin split  $\pi$  peaks. In Fig. 6(c) for spectrum with  $k_x = 1.69 \text{ \AA}^{-1}$  only one peak of Pt and two  $\pi$  peaks are presented close to the Fermi level. The branches  $\alpha$  and  $\beta$  in this region are located at binding energies around 1 and 1.5 eV, respectively.

#### IV. DISCUSSION

In previous studies [16,31,32], graphene synthesized on Pt(111) was considered as quasifreestanding graphene. The branch of the  $\pi$  state of graphene reaches the Fermi level and crosses it near the  $\bar{K}$  point of the BZ (see Figs. 3 and 5). In accordance with such a conclusion, Fig. 5(a) plots also the linearlike character of the graphene  $\pi$ -state dispersion and formation of the Dirac-cone states with the Dirac point located slightly above the Fermi level. Our estimations, based on the experimental measurements, give a value of about 150 meV shift of the Dirac point above the Fermi level. For contact of graphene with Pt the first-principles calculations [37] and calculations based on difference in the work function [38] give the value of the Dirac cone shift of about 0.2–0.3 eV which is in accordance with our calculations. The authors of Refs. [37,38] considered a weak interaction of graphene with the Pt substrate (physisorptionlike interaction). However, in our experiment we have shown that the graphene/Pt interface is characterized by spin-dependent hybridization of graphene and Pt states, and the system cannot be described as physisorptionlike. Our experimental data and calculations confirm a strong

hybridization between graphene  $\pi$  and Pt  $5d$  states with a corresponding spin-dependent avoided-crossing effect leading to significant distortions of the dispersion relations despite the preservation of a weak interaction with the substrate.

Moreover, this hybridization and the corresponding spin-dependent avoided-crossing effects between the Pt  $5d$  and graphene  $\pi$  states lead to the formation of a rich spin structure at the graphene/Pt interface with enhanced spin-orbit splitting of the graphene  $\pi$  states at the Fermi level. Here, it is noteworthy that the significant modification of the spin structure is not only taking place in the region of intersection between the branches of the Pt  $5d$  and graphene  $\pi$  states. The inversion of the spin polarization of the Pt  $5d$  states relative to the  $\bar{M}$  point of the SBZ of Pt(111) located at  $k_x = 1.3 \text{ \AA}^{-1}$  can be distinguished in the theoretical and experimental spin structures presented in Figs. 3 and 6, respectively. This inversion is related to the inversion in the spin polarization at points of high symmetry which is expected in systems with strong spin-orbit interaction. Comparing the spin polarization of the Pt  $5d$  states near the Fermi level in Fig. 6(b), one can clearly see the inversion of the Pt  $5d$  states in the spectra measured at  $k_x = 1.18 \text{ \AA}^{-1}$  and  $k_x = 1.40 \text{ \AA}^{-1}$ , i.e., at both sides of the  $\bar{M}$  point of the SBZ of Pt (lower and higher in  $k_x$  than the  $\bar{M}$  point). Modifications in the structure of the circular dichroism dispersions [difference profile in Fig. 4(b)] with opposite direction of the circular polarizations under crossing of the  $\bar{M}$  point of the Pt SBZ correlate well with the change of the sign of spin polarization in the spin structure. It is interesting that due to the  $\pi$ - $d$  hybridization the same inversion of the sign of the spin polarization can be distinguished for the graphene  $\pi$  states, as well. Comparing the spin polarization of the graphene  $\pi$  states at both sides of  $\bar{M}$  point of the SBZ of Pt in Fig. 6(b), measured at the same  $k_x = 1.18 \text{ \AA}^{-1}$  and  $k_x = 1.40 \text{ \AA}^{-1}$ , we can distinguish also the pronounced inversion of the sign of the spin polarization. Thus, the  $\bar{M}$  point of the SBZ of Pt appears as a high-symmetry point for both Pt  $5d$  and graphene  $\pi$  states.

We have to note that the observed modification of the spin structure of the graphene/Pt system in the region of the Dirac point of the graphene  $\pi$  states (the  $\bar{K}$  point of the graphene BZ) is determined by the spin-dependent avoided-crossing effects between Pt  $5d$  and graphene  $\pi$  states. This situation is similar to the case of the graphene/Au system [11] or graphene/Ir(111) [14], however, significant differences in the spin structure of these systems can be distinguished owing to energy positions of the valence Au, Ir, and Pt  $d$  states relative to the Fermi level. The Au  $d$  states are located far from the Fermi level at the  $\bar{K}$  point (the BE of the Au  $5d$  states is higher than 2.5 eV). Therefore, the main modification of the spin structure of the graphene/Au system caused by spin-dependent hybridization between graphene  $\pi$  and Au  $d$  states takes place at BEs higher than 2.5 eV. The schematic presentation of the formed spin structure is shown in Fig. 7(a). In the region of linear dispersion of the graphene  $\pi$  states near the  $\bar{K}$  point the influence of the avoided-crossing effect is significantly less without substantial distortion of the spin structure of the Dirac cone. In this case the spin-orbit splitting of the graphene  $\pi$  states in the region of the  $\bar{K}$  point (of about 100 meV) is mainly determined by the Rashba interaction caused by the high inner-atomic potential gradient at the

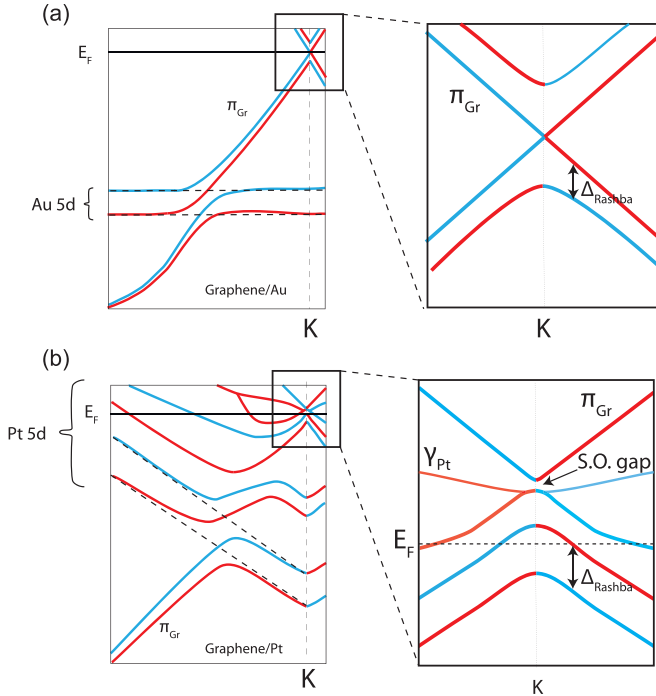


FIG. 7. (Color online) Schematic spin structure of the electronic states in graphene near the  $\bar{K}$  point for various graphene-contained systems. (a) Graphene with Rashba splitting, for example MG/Au/Ni(111). A hybridization of the Au  $d$  and graphene  $\pi$  states takes place below the Fermi level. (b) MG/Pt(111); a hybridization occurs in the region of the Dirac point and the Fermi level. Blue and red colors correspond to opposite spin polarizations.

graphene-Au interface whose influence is enhanced by the Au  $d$ -graphene  $\pi$ -state hybridization. The schematic illustration of the spin structure formed for the Dirac cone of graphene  $\pi$  and  $\pi^*$  states near the Dirac point is shown in the inset in Fig. 7(a) taken from Ref. [11]. The spin structure of graphene on Ir(111) is characterized by a similar behavior: the  $\pi$  state of graphene near the  $\bar{K}$  point lies in the local gap in the electronic structure of Ir. This type of spin structure and spin-orbit splitting of the graphene  $\pi$  states is expected for a system with Rashba spin-orbit splitting. It is related to the strong spin-orbit interaction with the substrate. Schematically such a structure can be constructed by *symmetrical* mirror reflection of the spin structure of the lower and upper Dirac cone, consisting of two oppositely spin-polarized cones. This spin structure is typical for the Rashba system with linear dispersion of electronic states.

However, due to the presence of Pt 5d states near the Fermi level in the region of the Dirac point and significant spin-dependent avoided-crossing effects between Pt and graphene states, the spin structure of the graphene/Pt system is significantly complicated. Figure 7(b) represents a schematic dispersion of the Pt 5d and graphene  $\pi$  states near the Dirac point, where the spin-dependent hybridization between Pt  $d$  and graphene  $\pi$  states and corresponding spin-dependent avoided-crossing effect leading to the modification of the spin structure near the Fermi level are shown. One of the results is the formation of enhanced spin-orbit splitting of graphene  $\pi$  states at the Fermi level. The value of the spin splitting is

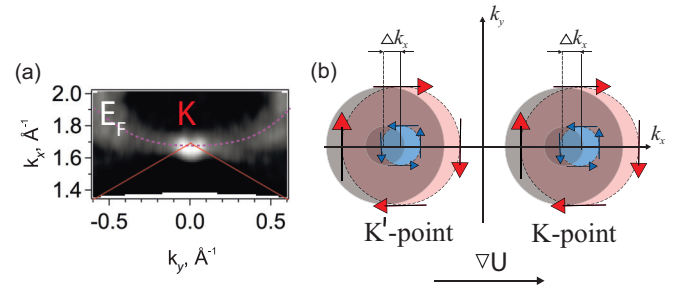


FIG. 8. (Color online) (a) Map of the states at the Fermi level near  $\bar{K}$  point of graphene, taken by using nonpolarized He I radiation. Purple line represents Pt  $d$  state, red solid line shows borders of the first Brillouin zone. (b) The difference between the contributions to the excited current of electrons with opposite spin orientations realized when setting up an electrical gradient between the ends of the system. The spin current developed in the graphene/Pt stripe due to an applied electrical or thermal gradient is characterized by the spin strongly locked perpendicular to the momentum of the moving electrons.

about 80–200 meV depending on the direction in the BZ. Furthermore, one can see from the calculations presented in Figs. 3(c) and 5(c) in the region of the Dirac point of graphene an additional intersection with the branch of the Pt  $d$  states. A corresponding spin-dependent avoided-crossing effect results in the formation of one nondegenerated branch with certain spin orientation in the region below the Dirac point. In the region above the Dirac point a nondegenerated branch with opposite orientation of spin appears. This spin structure near the Dirac point is *antisymmetric* with respect to the lower and upper Dirac cone relative to the Dirac point. This is rather similar to topological surface states; see for instance Refs. [39–41]. It differs principally from the dispersions presented in Fig. 7(a) characterized for the graphene/Au interface. Moreover, detailed theoretical analysis of the electronic structure of graphene on Pt(111) predicts the existence of the energy gap between upper and lower Dirac cones, with a value of 50 meV. Formation of the gap between the  $\pi$  and  $\pi^*$  states is the result of hybridization of the  $\pi$  states with the spin-orbit split  $d$  states of Pt. Such a type of the spin structure promises to offer a good perspective with respect to spintronics

However, let us come back to the spin structure formed at the Fermi level. Figure 8(a) represents the experimental map of the states at the Fermi level of graphene on Pt(111) near the  $\bar{K}$  point of graphene. Besides the ringlike  $\pi$  state of graphene at the  $\bar{K}$  point we can clearly see the branch of Pt  $d$  states, which passes through the ring of the graphene  $\pi$  state. This intersection leads to an opportunity of effective injection of spin current between graphene and Pt states. Additionally, hybridization between these states gives rise to anisotropic spin splitting of the graphene  $\pi$  state at the Fermi level. Taking into account the experimentally confirmed enhanced spin-orbit splitting of the graphene  $\pi$  states at the Fermi level and the availability of the spin-polarized Pt  $d$  states at the Fermi level in the region of the  $\bar{K}$  point of graphene one can use the graphene/Pt interface as a generator of spin current. This spin current should be characterized by

the in-plane orientation of spin strongly locked perpendicular to the momentum of moving electron. In Fig. 8(b), a schematic diagram of the Fermi surface for this system is presented in the regions of the  $\bar{K}$  and  $\bar{K}'$  point of the graphene BZ with the spin-split Dirac states showing the enhanced spin-orbit splitting (80–200 meV). If an electric field is applied along the interface, this spin-orbit splitting between the graphene  $\pi$  states can lead to an uncompensated spin accumulation and creation of a corresponding spin current along the applied electrical field. In Ref. [42] the authors showed that taking into account the experimental spin-orbit splitting of the graphene  $\pi$  states at the Fermi level of 80 meV the ratio of the spin and electrical currents in graphene/Pt(111) can be estimated on the level ( $|j_s|/|j_x| = 0.015$ ) that is comparable to those excited in other Pt-derived systems due to the spin Hall effect. Spin current, formed at the graphene/Pt interface can be used for remagnetization of magnetic nanodots, arranged atop the graphene/Pt system; for more details see Ref. [42]. More detailed analysis of spin current requires us to take into account the details of spin-dependent hybridization of states, such as anisotropy of splitting and deviation from linear dispersion.

The analysis of the spin current and application in spintronics of the graphene/Pt(111) described before includes only the Rashba splitting of the  $\pi$  states of graphene, because the Dirac point and topological-like features of the hybrid states are located above the Fermi level.

The appearance of a spin-orbit gap in graphene is intensively discussed, for instance, under the influence of heavy impurity atoms on graphene [43] or for transition-metal intercalated graphene [44]. It was shown that hybridization of the  $d$  states of heavy atoms with the  $\pi$  states can lead to a topological spin-orbit gap in the electronic structure. In Ref. [45] it was predicted that if the intrinsic spin-orbit interaction in graphene is stronger than the Rashba coupling, graphene assumes the topological insulator phase. Such a system is characterized by the quantum spin Hall effect and formation of topological edge states. These effects demand further detailed investigations. Because the Dirac point in the graphene/Pt(111) system is located above the Fermi level we cannot confirm experimentally the formation of such a spin structure. However, DFT calculations of the spin structure near the Dirac cone (see Figs. 3 and 5) show the formation of a gap between lower and upper cones, caused by spin-dependent hybridization.

## V. CONCLUSIONS

As a result of our investigation the following points have been established:

Electronic and spin structure of graphene synthesized by cracking of propylene on Pt(111) is characterized by linear dispersion of the graphene  $\pi$  states in the region of the  $\bar{K}$  point of the BZ both in the  $\bar{\Gamma}\bar{K}$  and perpendicular to the  $\bar{\Gamma}\bar{K}$  directions with the Dirac point position of 150 meV above the Fermi level.

Furthermore, due to the hybridization between the graphene  $\pi$  and Pt  $5d$  states the distortion of the dispersions including some local breaks in the region of their intersections are observed. Utilizing of  $p$ ,  $s$ , and elliptic polarization of the incident synchrotron radiation the contributions of the different states were separated and avoid-crossing effects between spin-orbit split Pt  $d$  states and graphene  $\pi$  state were established. The hybridization is followed by corresponding modification of the spin structure and appearance of enhanced induced spin-orbit splitting of the graphene  $\pi$  states. In the region of the Fermi level the magnitude of the spin splitting reaches 80–200 meV depending on the direction in the BZ. DFT calculations of the electronic and spin structures show a good agreement with the experimental data for the region of occupied states. Based on theoretical results, it was shown that the hybridization of the Pt and graphene states leads to formation of a unique non-Rashba spin structure of the Dirac cone, and even the appearance of a spin-orbit gap between the upper and lower cones.

## ACKNOWLEDGMENTS

We thank O. Rader for many useful discussions and for providing the samples for the experiments. The work was partially supported by a grant of Saint Petersburg State University for scientific investigations (Grant No. 11.38.271.2014) and Russian Foundation for Basic Research (RFBR) projects (Project No. 13-02-91327) and performed within the framework of collaboration between the Deutsche Forschungs-gemeinschaft and Russian Foundation for Basic Research (Grant No. RA 1041/3-1). We acknowledge the financial support of the University of Basque Country UPV/EHU (Grant No. GIC07-IT-756-13), the Departamento de Educacion del Gobierno Vasco and the Spanish Ministerio de Ciencia e Innovacion (Grant No. FIS2010-19609-C02-01), Project FIS2013-48286-C2-1-P of the Spanish Ministry of Economy and Competitiveness MINECO, and the Tomsk State University Competitiveness Improvement Program. The calculations were performed on the SKIF-Cyberia supercomputer at Tomsk State University (Russia). The authors also acknowledge support from the Russian-German laboratory at BESSY II and the “German-Russian Interdisciplinary Science Center” (G-RISC) program.

- 
- [1] K. S. Novoselov, A. K. Geim, S. V. Morozov, D. Jiang, M. I. Katsnelson, I. V. Grigorieva, S. V. Dubonos, and A. A. Firsov, *Nature (London)* **438**, 197 (2005).  
 [2] A. K. Geim and K. S. Novoselov, *Nat. Mater.* **6**, 183 (2007).  
 [3] A. H. Castro Neto, F. Guinea, N. M. R. Peres, K. S. Novoselov, and A. K. Geim, *Rev. Mod. Phys.* **81**, 109 (2009).

- [4] M. I. Katsnelson, K. S. Novoselov, and A. K. Geim, *Nat. Phys.* **2**, 620 (2006).  
 [5] N. Tombros, C. Jozsa, M. Popinciuc, H. T. Jonkman, and B. J. van Wees, *Nature (London)* **448**, 571 (2007).  
 [6] N. Tombros, S. Tanabe, A. Veligura, C. Jozsa, M. Popinciuc, H. T. Jonkman, and B. J. van Wees, *Phys. Rev. Lett.* **101**, 046601 (2008).

- [7] C. Józsa, M. Popinciuc, N. Tombros, H. T. Jonkman, and B. J. van Wees, *Phys. Rev. B* **79**, 081402 (2009).
- [8] A. A. Rybkina, A. G. Rybkin, V. K. Adamchuk, D. Marchenko, A. Varykhalov, J. S. Barriga, and A. M. Shikin, *Nanotechnology* **24**, 295201 (2013).
- [9] M. Popinciuc, C. Józsa, P. J. Zomer, N. Tombros, A. Veligura, H. T. Jonkman, and B. J. van Wees, *Phys. Rev. B* **80**, 214427 (2009).
- [10] A. M. Shikin, A. G. Rybkin, D. Marchenko, A. A. Rybkina, M. R. Scholz, O. Rader, and A. Varykhalov, *New J. Phys.* **15**, 013016 (2013).
- [11] D. Marchenko, A. Varykhalov, M. Scholz, G. Bihlmayer, E. Rashba, A. Rybkin, A. Shikin, and O. Rader, *Nat. Commun.* **3**, 1232 (2012).
- [12] A. Varykhalov, J. Sánchez-Barriga, A. M. Shikin, C. Biswas, E. Vescovo, A. Rybkin, D. Marchenko, and O. Rader, *Phys. Rev. Lett.* **101**, 157601 (2008).
- [13] M. Papagno, P. Moras, P. M. Sheverdyeva, J. Doppler, A. Garhofer, F. Mittendorfer, J. Redinger, and C. Carbone, *Phys. Rev. B* **88**, 235430 (2013).
- [14] D. Marchenko, J. Sánchez-Barriga, M. R. Scholz, O. Rader, and A. Varykhalov, *Phys. Rev. B* **87**, 115426 (2013).
- [15] A. B. Preobrajenski, M. L. Ng, A. S. Vinogradov, and N. Mårtensson, *Phys. Rev. B* **78**, 073401 (2008).
- [16] P. Sutter, J. T. Sadowski, and E. Sutter, *Phys. Rev. B* **80**, 245411 (2009).
- [17] G. Y. Guo, S. Murakami, T.-W. Chen, and N. Nagaosa, *Phys. Rev. Lett.* **100**, 096401 (2008).
- [18] H. Kontani, M. Naito, D. S. Hirashima, K. Yamada, and J.-i. Inoue, *J. Phys. Soc. Jpn.* **76**, 103702 (2007).
- [19] K. Uchida, S. Takahashi, K. Harii, J. Ieda, W. Koshibae, K. Ando, S. Maekawa, and E. Saitoh, *Nature (London)* **455**, 778 (2008).
- [20] T. Kimura, Y. Otani, T. Sato, S. Takahashi, and S. Maekawa, *Phys. Rev. Lett.* **98**, 156601 (2007).
- [21] I. Mihai Miron, G. Gaudin, S. Auffret, B. Rodmacq, A. Schuhl, S. Pizzini, J. Vogel, and P. Gambardella, *Nat. Mater.* **9**, 230 (2010).
- [22] D. Ralph and M. Stiles, *J. Magn. Magn. Mater.* **320**, 1190 (2008).
- [23] D. Marchenko, A. Varykhalov, M. R. Scholz, J. Sánchez-Barriga, O. Rader, A. Rybkina, A. M. Shikin, T. Seyller, and G. Bihlmayer, *Phys. Rev. B* **88**, 075422 (2013).
- [24] G. Kresse and J. Hafner, *Phys. Rev. B* **48**, 13115 (1993).
- [25] G. Kresse and J. Furthmüller, *Comput. Mater. Sci.* **6**, 15 (1996).
- [26] P. E. Blöchl, *Phys. Rev. B* **50**, 17953 (1994).
- [27] G. Kresse and D. Joubert, *Phys. Rev. B* **59**, 1758 (1999).
- [28] J. P. Perdew, K. Burke, and M. Ernzerhof, *Phys. Rev. Lett.* **77**, 3865 (1996).
- [29] D. D. Koelling and B. N. Harmon, *J. Phys. C* **10**, 3107 (1977).
- [30] S. Grimme, *J. Comput. Chem.* **27**, 1787 (2006).
- [31] M. Gao, Y. Pan, L. Huang, H. Hu, L. Z. Zhang, H. M. Guo, S. X. Du, and H.-J. Gao, *Appl. Phys. Lett.* **98**, 033101 (2011).
- [32] G. Otero, C. González, A. L. Pinaridi, P. Merino, S. Gardonio, S. Lizzit, M. Blanco-Rey, K. Van de Ruit, C. F. J. Flipse, J. Méndez *et al.*, *Phys. Rev. Lett.* **105**, 216102 (2010).
- [33] W. Di, K. E. Smith, and S. D. Kevan, *Phys. Rev. B* **45**, 3652 (1992).
- [34] E. Frantzeskakis, S. Pons, A. Crepaldi, H. Brune, K. Kern, and M. Grioni, *Phys. Rev. B* **84**, 245443 (2011).
- [35] A. Popova, A. Shikin, A. Rybkin, D. Marchenko, O. Vilkov, A. Makarova, A. Varykhalov, and O. Rader, *Phys. Solid State* **53**, 2539 (2011).
- [36] A. M. Shikin, G. V. Prudnikova, V. K. Adamchuk, F. Moresco, and K.-H. Rieder, *Phys. Rev. B* **62**, 13202 (2000).
- [37] C. Gong, G. Lee, B. Shan, E. M. Vogel, R. M. Wallace, and K. Cho, *J. Appl. Phys.* **108**, 123711 (2010).
- [38] G. Giovannetti, P. A. Khomyakov, G. Brocks, V. M. Karpan, J. van den Brink, and P. J. Kelly, *Phys. Rev. Lett.* **101**, 026803 (2008).
- [39] M. Z. Hasan and C. L. Kane, *Rev. Mod. Phys.* **82**, 3045 (2010).
- [40] D. Hsieh, Y. Xia, D. Qian, L. Wray, J. H. Dil, F. Meier, J. Osterwalder, L. Patthey, J. G. Checkelsky, N. P. Ong *et al.*, *Nature (London)* **460**, 1101 (2009).
- [41] A. M. Shikin, I. I. Klimovskikh, S. V. Eremeev, A. A. Rybkina, M. V. Rusinova, A. G. Rybkin, E. V. Zhizhin, J. Sánchez-Barriga, A. Varykhalov, I. P. Rusinov *et al.*, *Phys. Rev. B* **89**, 125416 (2014).
- [42] A. M. Shikin, A. A. Rybkina, A. G. Rybkin, I. I. Klimovskikh, P. N. Skirdkov, K. A. Zvezdin, and A. K. Zvezdin, *Appl. Phys. Lett.* **105**, 042407 (2014).
- [43] J. Hu, J. Alicea, R. Wu, and M. Franz, *Phys. Rev. Lett.* **109**, 266801 (2012).
- [44] Y. Li, P. Tang, P. Chen, J. Wu, B.-L. Gu, Y. Fang, S. B. Zhang, and W. Duan, *Phys. Rev. B* **87**, 245127 (2013).
- [45] C. L. Kane and E. J. Mele, *Phys. Rev. Lett.* **95**, 226801 (2005).